Eur. Phys. J. Spec. Top. (2026) 235:9357–9366
https://doi.org/10.1140/epjs/s11734-026-02392-x

THE EUROPEAN PHYSICAL JOURNAL SPECIAL TOPICS

Regular Article

Finite-time recurrence network transitivity in the ergodic limiter tokamak map

Matheus S. Palmero[1,2,a] and Reik V. Donner[1,3]

[1] Research Department IV – Complexity Science, Potsdam Institute for Climate Impact Research (PIK) – Member of the Leibniz Association, Potsdam, Germany
[2] Institute of Mathematics and Computer Sciences, University of São Paulo, São Paulo, Brazil
[3] Department of Water, Environment, Construction and Safety, Magdeburg–Stendal University of Applied Sciences, Magdeburg, Germany

Received 31 January 2026 / Accepted 18 May 2026 / Published online 10 June 2026
© The Author(s) 2026

Abstract Hamiltonian maps are a useful tool for modeling the magnetic field configuration in plasma fusion devices, such as tokamaks, particularly for understanding the complex topology created by magnetic perturbations. This work uses recurrence analysis, specifically the concept of recurrence network transitivity, to provide a quantitative characterization of the phase space in the ergodic limiter map, also known as the Ullmann map (UM). We generate recurrence network representations of finite-time example trajectories of this map with different initial conditions and estimate their respective transitivity for different magnetic perturbation strengths, demonstrating that this measure effectively identifies dynamically distinct regions based on their local geometric clustering. We observe marked bands of elevated finite-time transitivity embedded within the chaotic sea, indicating regions of reduced effective transient dimensionality. These highly structured zones in phase space are characteristic of trajectories trapped near partial transport barriers (cantori), making them spatially consistent with sticky dynamics. We also find that trajectories near unstable periodic orbits (UPOs) exhibit exceptionally high transitivity, offering new insights into the local structure of chaotic saddles. This recurrence network-based approach provides a quantitative, data-driven analysis of phase space structures in Hamiltonian systems, being also relevant for the understanding of plasma transport and magnetic confinement in tokamaks.

1 Introduction

Hamiltonian maps are often employed to model magnetic field-line configurations in tokamaks, a magnetic confinement device designed to produce controlled nuclear fusion [1–4]. This approach is physically grounded in the divergence-free condition of the magnetic field ($\nabla \cdot \vec{B} = 0$), which ensures that the dynamical system used to model the field lines is volume-preserving and, thus, inherently Hamiltonian. These models are particularly useful for investigating the effects of magnetic perturbations, whether intentionally introduced (e.g., by ergodic magnetic limiters) or arising from intrinsic plasma instabilities. The resulting phase space of the map provides a poloidal cross-section that models the magnetic configuration of the system, revealing complex structures, including invariant (KAM) curves, stability islands, and chaotic regions.

The focus here is on the ergodic limiter map, also known as the Ullmann map (UM) [5], which models the magnetic field configuration in tokamaks equipped with an ergodic limiter [6]. Although the phase space of this map exhibits a rich, mixed structure of regular and chaotic dynamics, qualitative visual inspection is often insufficient for a rigorous quantification of these regions. Consequently, several recent approaches [7–9] have been developed to investigate these regions of interest, particularly with respect to magnetic confinement and transport properties.

Despite the growing use of recurrence-based techniques in non-linear time-series analysis, their application to Hamiltonian systems have remained comparatively limited so far. Only a small number of studies have explicitly explored how recurrence analysis and related complex-network measures can distinguish between regular and chaotic motion in area-preserving systems, most notably in the context of the standard map [10–16]. In many of

[a] e-mail: palmero@usp.br (corresponding author)

these works, the recurrence rate (RR), i.e. the total fraction of pairs of state vectors considered recurrent, has been kept fixed, while the recurrence threshold ε has been adjusted adaptively. Although this facilitates comparisons between trajectories with different local densities, it effectively blends different spatial scales across phase space. Zou et al. [12] discussed both this setting and the complementary alternative of fixing ε and allowing RR to vary. In the present study, we explicitly adopt the latter approach. This choice enables the investigation of the dynamics at a uniform spatial scale, which is particularly relevant for magnetic field-line systems where transport and confinement properties are governed by geometric structures in phase space.

In this work, we address the gap in our understanding of the phase space structure by introducing a complementary, data-driven approach to characterize trajectories emanating from different initial conditions. While variational chaos indicators (such as Lyapunov exponents or SALI) [17–19] are excellent tools for systems where the equations of motion and the tangent map are explicitly known, they primarily measure local expansion and contraction rates. Here, we employ methods from recurrence analysis, specifically the concept of finite-time network transitivity, to differentiate between different dynamical regimes based purely on simulated trajectories. This measure, derived from the recurrence matrix, provides a quantitative assessment of the effective transient dimensionality and, hence, geometry of an orbit. By applying this strictly data-driven measure to the UM, we aim to demonstrate how transitivity patterns can successfully map the underlying phase space features. In particular, we show how transitivity highlights regions of dense spatial organization that are structurally characteristic of trajectories trapped near partial transport barriers, commonly referred to as sticky zones. This offers a complementary perspective to traditional variational methods and lays the groundwork for future applications in experimental or computationally complex tokamak plasmas where tangent maps are unavailable.

2 The model

Models for tokamak magnetic fields often draw inspiration from established area-preserving maps, such as the Chirikov standard map [20]. The equilibrium configuration $\vec{B}^0$ is formed by the superposition of a poloidal field B_θ, generated by a toroidal plasma current, and a strong toroidal field B_ϕ. This equilibrium can be described by a generating function $G(r_{n+1}, \theta_n)$ for the magnetic field lines.

The plasma current density $\vec{J}$ is typically modeled as

$$\vec{J} = j_0 \left(1 - \frac{r^2}{a^2}\right)^\gamma \Theta(a - r)\hat{z} \ , \tag{1}$$

where j_0 and γ are adjustable parameters, a is the plasma column radius, and $\Theta(\cdot)$ is the Heaviside step function.

The map for the magnetic field lines can be derived from a generating function

$$G(r_{n+1}, \theta_n) = r_{n+1}\theta_n + 2\pi \int^{r_{n+1}} \iota(r')\mathrm{d}r' \ , \tag{2}$$

where $\iota(r)$ is the winding number. This is related to the safety factor $q(r)$, a crucial parameter in tokamak physics, by

$$q(r) \equiv \frac{1}{\iota(r)} \ . \tag{3}$$

A rational safety factor $q = M/N$ corresponds to a closed field line on a rational surface. By contrast, an irrational q leads to a field line that densely fills an invariant (KAM) surface [21, 22]. The equilibrium safety factor $q^0(r)$ is derived from the current density profile in Eq. (1):

$$q^0(r) = q_a \frac{r^2}{a^2} \left[1 - \left(1 - \frac{r^2}{a^2}\right)^{\gamma+1} \Theta(a - r)\right]^{-1} \ , \tag{4}$$

where q_a is the safety factor at the plasma edge ($r = a$).

This generating function leads to the unperturbed map

$$\begin{cases} r_{n+1} = r_n \\ \theta_{n+1} = \theta_n + 2\pi/q^0(r_{n+1}) \end{cases} \ . \tag{5}$$

Toroidal corrections, accounting for the Shafranov shift [23], are introduced via an additional term in the generating function. Keeping the first-order term ($a_1 = -0.04$) yields the unperturbed Ullmann map given by

$$\begin{cases} r^*_{n+1} = \frac{r_n}{1-a_1\sin(\theta_n)} \\ \theta^*_{n+1} = \theta_n + \frac{2\pi}{q^0(r_{n+1})} + a_1\cos(\theta_n) \end{cases} . \tag{6}$$

A perturbation from an external ergodic limiter is then added. This is described by a perturbed generating function

$$G_{\text{pert}}(r_{n+1}, \theta_n) = r_{n+1}\theta_n - \frac{C}{m-1}\left(\frac{r_{n+1}}{b}\right)^{m-1}\cos(m\theta_n) , \tag{7}$$

where b is the tokamak minor radius, m is the perturbation mode (number of limiter current loops), and C is the perturbation strength. This results in the perturbed component of the map

$$\begin{cases} r_n = r^*_{n+1} + \frac{mb}{m-1}C\left(\frac{r^*_{n+1}}{b}\right)^{m-1}\sin(m\theta^*_n) \\ \theta_{n+1} = \theta^*_n - C\left(\frac{r^*_{n+1}}{b}\right)^{m-2}\cos(m\theta^*_n) \end{cases} . \tag{8}$$

Combining Eqs. (6) and (8) gives the full tokamak ergodic limiter map, or Ullmann map. The perturbation strength C is then related to the relative poloidal perturbation dB:

$$C = \frac{2\pi}{q_a}\left(\frac{b}{a}\right)^{m-2}\mathrm{d}B , \tag{9}$$

where $\mathrm{d}B = B_{ex}/B_\theta(a)$ is the control parameter in our simulations.

For this study, we use parameters corresponding to the Tokamak Chauffage Alfvén Brésilien (TCABR) [24] and set the perturbation mode $m = 7$. The phase space is represented in dimensionless coordinates $y = 1 - r/b$ and $x = \theta/2\pi$. The region $y > 0.5$ represents the confined inner plasma, while $y < 0.5$ is the outer, perturbed region. Figure 1 shows a typical phase space for $\mathrm{d}B = 1.0\%$.

As the perturbation dB increases, the chaotic region expands, as shown in Fig. 2. As a particular example, our study focuses on the region near the $m = 7$ island chain, visible around $y \approx 0.3$. This chain is critical as it separates confined regions from outer chaotic areas where field lines may escape [25].

The dynamics in this outer chaotic region are governed by stable and unstable manifolds of the unstable periodic orbits (UPOs) associated with the island chain. Figure 3 illustrates the phase space for $\mathrm{d}B = 1.5\%$, highlighting the $m = 7$ UPO and its unstable manifold. Trajectories in this region may follow the complex structure of the manifold, motivating a quantitative analysis beyond visual inspection.

Calculating the positions of UPOs and tracing manifolds are difficult tasks that can only be overcome using fitting numerical tools. In our results, we use the efficient method proposed by Ciro et al. [26] that, essentially, chooses an appropriate segment in a linear approximation for the dynamics and evolves said segment under the mapping and under its inverse.

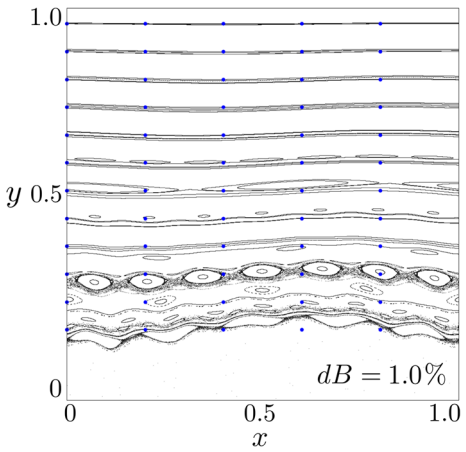


Fig. 1 Phase space of the UM for a relative poloidal magnetic field perturbation strength $\mathrm{d}B = 1.0\%$. The initial conditions set are depicted by the blue points

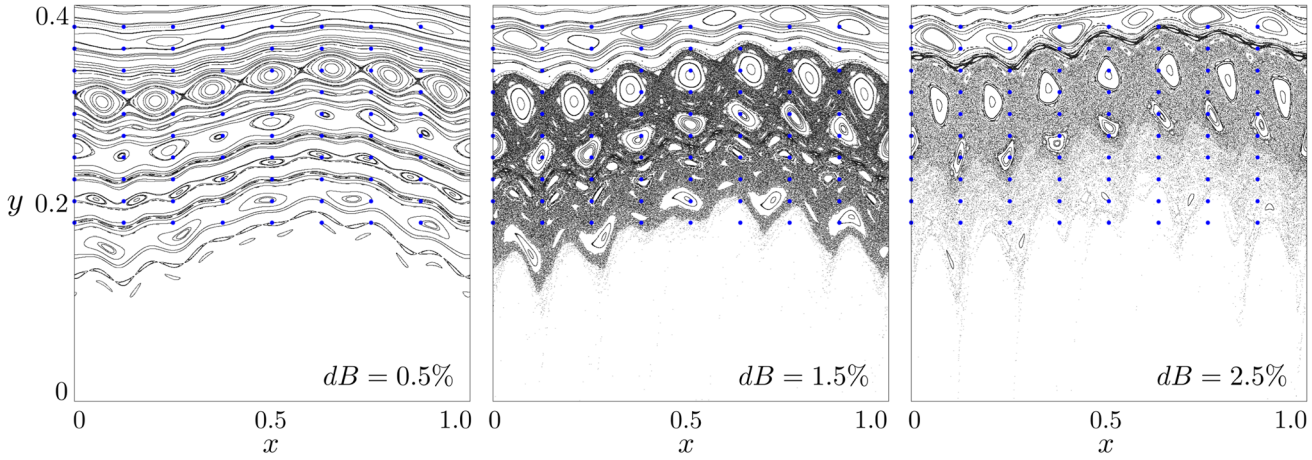


Fig. 2 Outer chaotic region of the phase spaces for three values of the relative perturbation dB. The initial conditions set are depicted by the blue points and will be kept the same for all following results

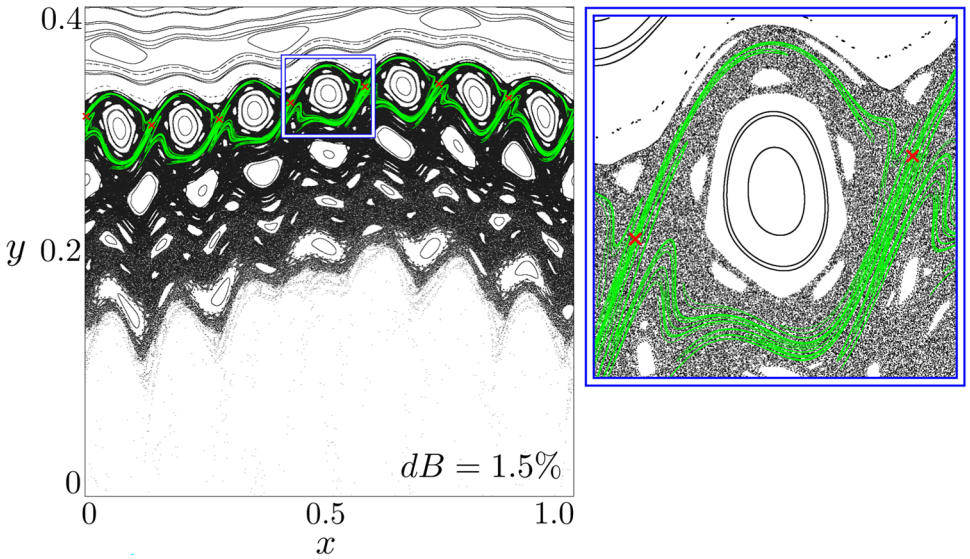


Fig. 3 Phase space for d$B = 1.5\%$. The period-7 UPO is marked by red x's, and its unstable manifold is shown in green. The blue frame shows a magnified view around one of the period-7 islands

3 Numerical methods

Recurrence is a fundamental property of dynamical systems, characterized by the tendency of a trajectory to return to the vicinity of previously visited regions of its phase space. For a trajectory $\{\vec{\psi}_i\}_{i=1}^{N}$, a state is considered recurrent if it returns to an ε-neighborhood of a prior state. This is formalized by the binary recurrence matrix (RM), with elements $R_{i,j}$ given by

$$R_{i,j}(\varepsilon) = \Theta(\varepsilon - \|\vec{\psi}_i - \vec{\psi}_j\|) \ , \tag{10}$$

where $\vec{\psi}_i$ and $\vec{\psi}_j$ represent the system states at times i and j, $\Theta(\cdot)$ is the Heaviside step function, $\|\cdot\|$ denotes a chosen norm, and ε is the recurrence threshold [27, 28].

In the present study, the state vectors are taken directly as $\vec{\psi}_i = (x_i, y_i) \in \mathbb{R}^2$, corresponding to the dimensionless phase space coordinates of the map, without delay embedding. Distances in Eq. (10) are therefore computed in the two-dimensional phase space using the Euclidean norm. For the recurrence analysis, we restrict the dynamics to the outer chaotic region shown in Fig. 2, and linearly rescale this domain to the unit square to ensure comparability of distances.

As previously mentioned, the recurrence threshold is kept fixed in this work. Specifically, we will consistently use $\varepsilon = 0.05$. The choice of ε acts as a spatial scale of observation, defining the neighborhood size required to establish the recurrence network. If ε is too small, the network becomes disconnected, commonly resulting in a potentially

biased estimate of the network transitivity; if too large, it induces unnecessary links between distant regions and thereby blurs relevant information about the geometric fine structure of the trajectory. Here, the specific value of $\varepsilon = 0.05$ (corresponding to 5% of the width of the normalized phase space domain) was determined empirically. Through numerical testing, we found this value is large enough to prevent the finite-time recurrence network from fragmenting into disconnected sub-graphs, yet small enough to accurately resolve fine geometric structures without blurring them together, ensuring that the transitivity captures the selected dynamical regimes at a uniform spatial resolution. Furthermore, since the x-coordinate originates from a poloidal angle, it is treated as a periodic variable, and distances are evaluated using the minimum separation under 2π-periodicity.

Beyond traditional line-based quantification methods of the resulting recurrence plots [29], the RM can be interpreted as the adjacency matrix of a *recurrence network* (RN) [30]. In this framework, each state $\vec{\psi}_i$ is treated as a spatially embedded node, and an edge exists between nodes i and j if they are ε-close. This perspective integrates complex-network theory to objectively quantify the underlying dynamics. To analyze the network's structural characteristics, we define the adjacency matrix (AM) by removing self-loops via the Kronecker delta $\delta_{i,j}$, resulting in the matrix elements

$$A_{i,j}(\varepsilon) = R_{i,j}(\varepsilon) - \delta_{i,j} \ . \tag{11}$$

From the AM, we compute the network transitivity $\mathcal{T}$, which measures the global probability that two randomly chosen neighbors of any node are also connected (i.e., ε-close) to each other. It is defined as follows:

$$\mathcal{T} = \frac{3N_\Delta}{N_3} = \frac{\sum_{i,j,k;i\neq j\neq k} A_{ij}A_{ik}A_{jk}}{\sum_{i,j,k;i\neq j\neq k} A_{ij}A_{ik}} \ , \tag{12}$$

where N_Δ is the number of closed triangles (3-loops) and N_3 is the number of connected triples in the network.

It is important to note that the aforementioned network transitivity differs from the concept of topological transitivity, which describes the properties of continuous topological transformations. Instead, network transitivity refers to fundamental algebraic relationships between triples of discrete objects, measuring the relative fraction of triples where the binary linkage relationship between pairs of nodes is actually transitive. In graph-theoretical terms, we identify the set of states with the set of vertices V and the recurrence relation with the mutual adjacency of pairs. Thus, for a given vertex $i \in V$, transitivity implies that for two other vertices j, $k \in V$, if $A_{ij} = A_{ik} = 1$, then $A_{jk} = 1$ also holds. Characterizing the degree of transitivity, or the relative frequency of closed 3-loops, provides information on the structural graph properties, which are intrinsically linked to the local geometric complexity of the underlying dynamical system.

Since the state vectors are embedded in a two-dimensional metric space, geometric constraints impose characteristic bounds on the network transitivity. For random geometric graphs in two dimensions, transitivity is bounded from below by approximately 9/16, reflecting the probability of triangle formation in a homogeneous point cloud [31]. This value is also asymptotically exact for random geometric graphs defined using the maximum norm, but not for the Euclidean norm used here. Continuous trajectories exhibit characteristic values of recurrence network transitivity relative to this bound: $\mathcal{T} \approx 1$ for fixed points, $\mathcal{T} \approx 0.75$ for periodic orbits, and values approaching the random geometric limit for space-filling motion, with small deviations depending on the chosen norm.

For discrete maps, the situation differs because trajectories consist of jumps between separated states rather than continuous motion, which alters the geometric interpretation of transitivity. Recurrence network studies of low-dimensional maps nonetheless reveal systematic behavior across dynamical regimes. For dissipative chaotic systems such as the Hénon map, the global clustering coefficient (closely related to transitivity) typically lies in the range 0.72–0.78, depending on ε [30]. Analytical and numerical results for one-dimensional maps show comparable values: for the Bernoulli map, the global clustering coefficient can be derived analytically along with its dependence on the recurrence threshold ε, while for the fully chaotic logistic map ($r = 4$), values around 0.75–0.84 have been reported; periodic windows of the logistic map, in contrast, yield values approaching unity [30, 32]. Although global clustering coefficient and transitivity are not identical measures, they are closely related and display analogous trends. For the Chirikov standard map, another Hamiltonian area-preserving system, Zou et al. [12] found $\mathcal{T} \approx 0.6$ for space-filling chaotic motion, $\mathcal{T} \approx 0.75$ for periodic orbits, and even higher values for sticky trajectories near regular islands.

These results indicate that, despite quantitative differences arising from the metric and threshold choice, recurrence network transitivity consistently orders dynamical regimes according to their geometric organization in phase space, which is supported by its link with generalized notion of an effective fractal dimension for random geometric graphs on non-integer dimensional manifolds [31]. The behavior observed for the Ullmann map can therefore be interpreted in close analogy to that established for the standard map.

In our numerical investigations, the simulated trajectories $\{\vec{\psi}_i\}$ generated by the UM, Eqs. (6) and (8), are analyzed using the recurrence-based framework described above. For each finite-time trajectory, we first construct the binary RM ($R_{i,j}$) following Eq. (10), which is subsequently transformed into the AM ($A_{i,j}$), allowing for a

complex-network interpretation of the recurrences. Finally, the network transitivity $\mathcal{T}$ is calculated via Eq. (12). This procedure enables the objective quantification of the system's transitivity. As established by our choice of parameters, these recurrence matrix-based estimates of $\mathcal{T}$ provide finite-time and scale-local characteristics of each considered trajectory of interest.

4 Results and discussion

We first estimate the recurrence network transitivity $\mathcal{T}$ to visualize the spatial distribution of the different dynamical regimes across the phase space. Because the UM is a discrete area-preserving map, its iterations naturally form a Poincaré section. Therefore, rather than computing $\mathcal{T}$ over a dense spatial mesh of initial conditions, we utilize the exact same set of representative initial conditions previously depicted by the blue points in Fig. 2. Specifically, each of these initial conditions is evolved up to $N = 10^3$ iterations of the UM, and the respective RM is calculated using a fixed threshold $\varepsilon = 0.05$. A single transitivity value $\mathcal{T}$ is then computed for each finite-time trajectory. Every point along a given trajectory is assigned this corresponding scalar value, yielding the color-coded phase space portraits depicted in Fig. 4.

As we are performing a *finite-time* recurrence analysis, the $N = 10^3$ iterations provide a structural footprint of the short-term dynamics. Physically, $N = 10^3$ represents a relevant number of toroidal transits to capture short-term field-line confinement. For trajectories that might be trapped near magnetic islands or partial transport barriers, this specific time-scale allows $\mathcal{T}$ to resolve the internal connectivity of these structures before the trajectory eventually escapes and explores larger portions of the chaotic sea. If significantly shorter trajectories were used (e.g., $N \approx 500$) for the same value of ε, the resulting networks would be too sparse to reliably form the closed triangles necessary to compute $\mathcal{T}$. Conversely, for much longer trajectories (e.g., $N \approx 5000$), the eventual leak into the broader chaotic sea would wash out the local geometric footprint, causing $\mathcal{T}$ to drop toward the global space-filling limit and masking these transient structures. Consequently, the elevated transitivity values observed for these finite-time trapped trajectories should be interpreted with some care. Such values may reflect the structural coherence of motion constrained near invariant structures, but they could also arise if the trajectory samples a limited number of dense regions in phase space that remain only weakly interconnected. Since transitivity alone cannot discriminate between these scenarios, its interpretation must always be considered in tandem with the chosen spatial scale ε.

The transitivity maps depicted in Fig. 4 reveal distinct structures not easily discerned from the standard phase space plots shown in Fig. 2 at first glance. In particular, for weak magnetic perturbation ($\mathrm{d}B = 0.5\%$), the transitivity map is dominated by uniformly high values, reflecting the near-integrable nature of the dynamics and the predominance of quasi-periodic trajectories. In this regime, recurrences are strongly clustered along smooth invariant curves, leading to large values of $\mathcal{T}$ that are indicative of a low effective dimensionality of the motion [31].

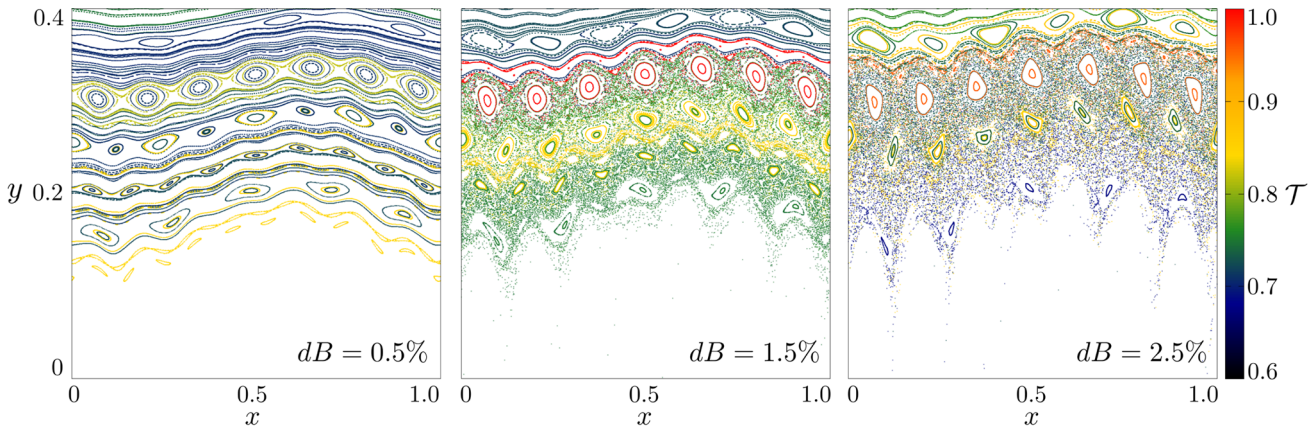


Fig. 4 Finite-time recurrence network transitivity $\mathcal{T}$ computed for the phase spaces shown in Fig. 2, considering $\varepsilon = 0.05$. All initial conditions, depicted in blue in Fig. 2, were evolved up to $N = 10^3$ iterations of the UM. The color scale is consistent for all three perturbation strengths

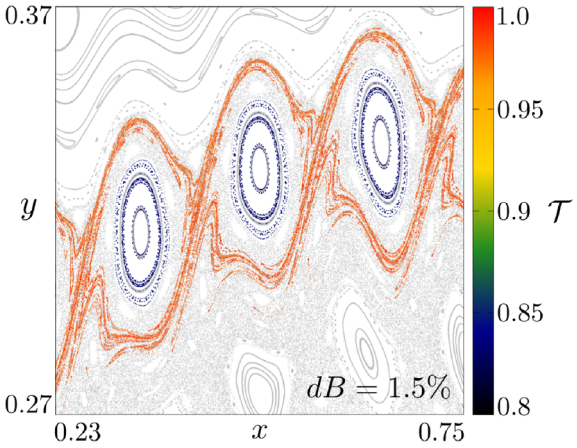


Fig. 5 Amplified phase space region for $dB = 1.5\%$. The transitivity $\mathcal{T}$ is shown for trajectories initiated near the stable periodic orbit (center) and in a small 10^{-12} box around the UPO

As the perturbation strength increases ($dB = 1.5\%$ and 2.5%), the transitivity maps exhibit more spatial heterogeneity associated with the progressive breakdown of invariant tori and the expansion of chaotic regions. Intermediate perturbation strengths reveal a mixed phase space, where elevated transitivity values persist inside surviving magnetic islands, while significantly lower values are observed in the chaotic sea. Notably, regions surrounding island boundaries often display intermediate transitivity values, which can be attributed to sticky dynamics, where trajectories remain temporarily trapped near regular structures before undergoing chaotic transport [33]. For the strongest perturbation, low transitivity values dominate, reflecting the exploration of chaotic regions by most of the evolved trajectories. In this strongly chaotic regime, the reduced clustering of recurrences captured by $\mathcal{T}$ provides a quantitative signature of enhanced chaos and radial transport.

To probe the transitivity measure in more detail, we analyzed two dynamically significant regions of the phase space for $dB = 1.5\%$: the vicinity of the period-7 stable periodic orbit at the center of a magnetic island; and the vicinity of the associated UPO. Figure 5 shows the transitivity $\mathcal{T}$ computed for two distinct ensembles of initial conditions. First, for the stable region, we placed a square of side length 0.025, centered at the stable periodic orbit, with 4×4 equally spaced initial conditions evolved for 100 iterations. For the unstable region, a very small square of side length 10^{-12}, centered at the previous calculated UPO position, was populated with 50×50 initial conditions, each also evolved up to 100 iterations.

While one might expect stable trajectories to exhibit larger transitivity values, we observe the opposite behavior: trajectories evolved from the vicinity of the UPO display consistently higher transitivity ($\mathcal{T} \approx 0.97$) than those associated with the stable orbit ($\mathcal{T} \approx 0.85$). This apparently counter-intuitive numerical observation can be understood by noting that transitivity reflects the local topological clustering of state vectors along the trajectory rather than its dynamical stability. The difference in $\mathcal{T}$ fundamentally stems from how the phase space geometry interacts with the ε-neighborhood. Near the stable periodic orbit (an elliptic point), the motion is confined to smooth, 1D invariant KAM curves. Within a local ε-neighborhood, the trajectory forms a simple arc, and the formation of network triangles is limited by the sequential, quasi-periodic jumps along this structure, yielding lower transitivity values.

In contrast, the vicinity of the UPO (a hyperbolic point) is governed by the homoclinic tangle of the stable and unstable manifolds. Because the unstable manifold folds infinitely upon itself, an ε-neighborhood near the UPO encapsulates multiple tightly packed, nearly parallel folds of the trajectory. Points across these different folds become mutually ε-close, creating highly dense clusters in the recurrence network. This massive increase in closed triangular connections drives the transitivity to higher values.

5 Conclusion and outlook

In this work, we have applied the concept of network transitivity, derived from recurrence analysis, to investigate the phase space structure of the ergodic limiter map. Our results demonstrate that the transitivity $\mathcal{T}$ provides a sensitive and geometrically meaningful quantitative measure for identifying and characterizing dynamically distinct regions of phase space. By mapping $\mathcal{T}$ over phase space for increasing magnetic perturbation strengths, we showed that this measure effectively captures the transition from near-integrable, laminar field-line motion to predominantly chaotic dynamics, while resolving mixed phase space structures such as magnetic islands, stochastic layers, and complex geometric zones that are not easily discerned from standard phase space visualizations alone.

A particularly important finding is the ability of transitivity to highlight regions of effectively lower-dimensional clustering embedded within the chaotic sea that can persist under increasing magnetic perturbations. Because

these topological signatures are characteristic of trajectories trapped near partial transport barriers (cantori), they are spatially consistent with sticky dynamics, indicating potential implications for plasma transport and confinement. At a more local level, the analysis of special trajectories revealed that field lines initiated in the immediate vicinity of an UPO exhibit high-transitivity values, even exceeding those associated with nearby stable periodic orbits. This observation highlights that network transitivity is primarily sensitive to the local geometric constraints and effective dimensionality imposed by invariant manifolds, rather than to dynamical stability itself. It also emphasizes the organizing role of unstable manifolds as low-dimensional skeletons guiding transport in chaotic magnetic configurations.

Despite these numerical observations, several open questions and limitations remain, which motivate further investigation. We point out three in particular:

- **Transport correlation:** A systematic study correlating network transitivity with transport properties, such as local diffusion coefficients, radial displacement statistics, or particle escape times, is suggested to quantitatively substantiate the interpretation of high-transitivity regions as partial transport barriers;
- **Parameter dependence:** The dependence of $\mathcal{T}$ on the recurrence threshold ε and the total iteration time N should be explored in detail in order to assess the robustness of the measure and optimize its application across different dynamical regimes;
- **UPO-related transitivity:** The unusually high transitivity observed near UPOs warrants further investigation. Clarifying how $\mathcal{T}$ relates to local Lyapunov exponents, manifold curvature, or the increased chaotic region for higher values of the control parameter could provide deeper insight into the microscopic organization of chaotic transport.

Overall, this work establishes finite-time recurrence network transitivity as a complementary tool for the analysis of transient complex dynamics in Hamiltonian systems. Beyond the ergodic limiter map, the approach presented here may be readily extended to more realistic magnetic field-line models and, potentially, to experimental data from tokamak dischargers, offering a novel framework for the study of stochastic transport and confinement properties in magnetically confined plasmas.

Acknowledgements M. S. Palmero acknowledges the São Paulo Research Foundation (FAPESP), project numbers 2024/22136-6, 2023/07704-5, 2020/12478-6, and 2018/03000-5. Most of the work presented in this paper was carried out during a visiting PhD period under the supervision of Prof. Iberê Caldas and Prof. Igor Sokolov, whom M. S. Palmero thanks for valuable discussions.

Author contributions

M.P.S. conceptualized the study, performed the numerical simulations, analyzed the data, and wrote the manuscript; R.V.D. revised the manuscript and contributed to the interpretation of the obtained results.

Funding Open Access funding enabled and organized by Projekt DEAL. São Paulo Research Foundation (FAPESP), project numbers 2024/22136-6, 2023/07704-5, 2020/12478-6, and 2018/03000-5.

Data availability The datasets generated during and/or analyzed during the current study are available via https://doi.org/10.5281/zenodo.20085012.

Materials availability Not applicable.

Code availability The custom code used for the simulations is available from the corresponding author on request.

Declarations

Conflict of interest The authors declare no conflict of interest.

Ethical approval and consent to participate Not applicable. This research does not involve human participants or animals.

Consent for publication Not applicable.

Open Access This article is licensed under a Creative Commons Attribution 4.0 International License, which permits use, sharing, adaptation, distribution and reproduction in any medium or format, as long as you give appropriate credit to the original author(s) and the source, provide a link to the Creative Commons licence, and indicate if changes were made. The images or other third party material in this article are included in the article's Creative Commons licence, unless

indicated otherwise in a credit line to the material. If material is not included in the article's Creative Commons licence and your intended use is not permitted by statutory regulation or exceeds the permitted use, you will need to obtain permission directly from the copyright holder. To view a copy of this licence, visit http://creativecommons.org/licenses/by/4.0/.

References

1. K.J. Whiteman, Invariants and stability in classical mechanics. Rep. Prog. Phys. **40**(9), 1033 (1977). https://doi.org/10.1088/0034-4885/40/9/002
2. P.J. Morrison, Magnetic field lines, Hamiltonian dynamics, and nontwist systems. Phys. Plasmas **7**, 2279–2289 (2000). https://doi.org/10.1063/1.874062
3. T.E. Evans, R.K.W. Roeder, J.A. Carter, B.I. Rapoport, Homoclinic tangles, bifurcations and edge stochasticity in diverted tokamaks. Contrib. Plasma Phys. **44**(1–3), 235–240 (2004). https://doi.org/10.1002/ctpp.200410034
4. R.L. Viana, M. Mugnaine, I.L. Caldas, Hamiltonian description for magnetic field lines in fusion plasmas: a tutorial. Phys. Plasmas **30**(9), 090901 (2023). https://doi.org/10.1063/5.0170345
5. K. Ullmann, I.L. Caldas, A symplectic mapping for the ergodic magnetic limiter and its dynamical analysis. Chaos Solitons Fractals **11**, 2129–2140 (2000). https://doi.org/10.1016/s0960-07799900138-1
6. T.J. Martin, J.B. Taylor, Ergodic behaviour in a magnetic limiter. Plasma Phys. Control. Fusion **26**(1B), 321 (1984). https://doi.org/10.1088/0741-3335/26/1B/005
7. S. Ahmadi, A. Salar Elahi, M. Ghorannevis, Structure of chaotic magnetic field lines in IR-T1 tokamak due to ergodic magnetic limiter. AIP Adv. **8**(3), 035302 (2018). https://doi.org/10.1063/1.5019789
8. M.S. Palmero, I.L. Caldas, Confining and escaping magnetic field lines in tokamaks: analysis via symplectic maps. Fundam. Plasma Phys. **8**, 100027 (2023). https://doi.org/10.1016/j.fpp.2023.100027
9. M. Mugnaine, I.L. Caldas, J.D. Szezech, R.L. Viana, Nontwist field line mapping in a tokamak with ergodic magnetic limiter. Phys. Rev. E **108**, 055206 (2023). https://doi.org/10.1103/PhysRevE.108.055206
10. Y. Zou, D. Pazó, M.C. Romano, M. Thiel, J. Kurths, Distinguishing quasiperiodic dynamics from chaos in short-time series. Phys. Rev. E **76**, 016210 (2007). https://doi.org/10.1103/PhysRevE.76.016210
11. Y. Zou, M. Thiel, M.C. Romano, J. Kurths, Characterization of stickiness by means of recurrence. Chaos: Interdiscip. J. Nonlinear Sci. **17**(4), 043101 (2007). https://doi.org/10.1063/1.2785159
12. Y. Zou, R.V. Donner, M. Thiel, J. Kurths, Disentangling regular and chaotic motion in the standard map using complex network analysis of recurrences in phase space. Chaos: Interdiscip. J. Nonlinear Sci. **26**(2), 023120 (2016). https://doi.org/10.1063/1.4942584
13. M.S. Santos, M. Mugnaine, J.D. Szezech Jr., A.M. Batista, I.L. Caldas, M.S. Baptista, R.L. Viana, Recurrence-based analysis of barrier breakup in the standard nontwist map. Chaos: Interdiscip. J. Nonlinear Sci. **28**(8), 085717 (2018). https://doi.org/10.1063/1.5021544
14. M.S. Palmero, I.L. Caldas, I.M. Sokolov, Finite-time recurrence analysis of chaotic trajectories in Hamiltonian systems. Chaos: Interdiscip. J. Nonlinear Sci. **32**(11), 113144 (2022). https://doi.org/10.1063/5.0102424
15. M.R. Sales, M. Mugnaine, J.D. Szezech Jr., R.L. Viana, I.L. Caldas, N. Marwan, J. Kurths, Stickiness and recurrence plots: an entropy-based approach. Chaos: Interdiscip. J. Nonlinear Sci. **33**(3), 033140 (2023). https://doi.org/10.1063/5.0140613
16. J. Daquin, T. Kovács, Leveraging temporal features of the divergence quantifier of recurrence plot to detect chaos in conservative systems. Eur. Phys. J. Spec. Top. **2026**, 1–19 (2026). https://doi.org/10.1140/EPJS/S11734-026-02183-4
17. G. Benettin, L. Galgani, A. Giorgilli, J.M. Strelcyn, Lyapunov characteristic exponents for smooth dynamical systems and for Hamiltonian systems; a method for computing all of them. Part 1: Theory. Meccanica **15**, 9–20 (1980). https://doi.org/10.1007/BF02128236
18. C. Skokos, C. Antonopoulos, T.C. Bountis, M.N. Vrahatis, Detecting order and chaos in Hamiltonian systems by the SALI method. J. Phys. A: Math. Gen. **37**, 6269 (2004). https://doi.org/10.1088/0305-4470/37/24/006
19. C. Skokos, The Lyapunov characteristic exponents and their computation, In *Dynamics of Small Solar System Bodies and Exoplanets*, ed. by J. Souchay, R. Dvorak. Lecture Notes in Physics, vol 790 (Springer, Berlin, Heidelberg, 2010). https://doi.org/10.1007/978-3-642-04458-8_2
20. B.V. Chirikov, Research concerning the theory of non-linear resonance and stochasticity. Technical report, CM-P00100691 (1969)
21. G.M. Zaslavsky, *Chaos in Dynamic Systems* (Harwood Academic Publishers, 1985)
22. I.L. Caldas, Shearless transport barriers in magnetically confined plasmas. Plasma Phys. Control. Fusion **54**(12), 124035 (2012). https://doi.org/10.1088/0741-3335/54/12/124035
23. V.D. Shafranov, Equilibrium of a toroidal pinch in a magnetic. Atomnaya Energiya **13**, 521–529 (1962). https://doi.org/10.1007/BF01312317
24. E.C. Silva, I.L. Caldas, Ergodic magnetic limiter for the TCABR. Braz. J. Phys. **32**, 39–45 (2002). https://doi.org/10.1590/S0103-97332002000100008
25. T. Kroetz, M. Roberto, E.C. Silva, I.L. Caldas, R.L. Viana, Escape patterns of chaotic magnetic field lines in a tokamak with reversed magnetic shear and an ergodic limiter. Phys. Plasmas **15**(9), 092310 (2008). https://doi.org/10.1063/1.2988335

26. D. Ciro, I.L. Caldas, R.L. Viana, T.E. Evans, Efficient manifolds tracing for planar maps. Chaos: Interdiscip. J. Nonlinear Sci. **28**(9), 093106 (2018). https://doi.org/10.1063/1.5027698
27. J.P. Eckmann, O.O. Kamphorst, D. Ruelle, Recurrence plots of dynamical systems. Europhys. Lett. **4**, 973 (1987). https://doi.org/10.1209/0295-5075/4/9/004
28. N. Marwan, M.C. Romano, M. Thiel, J. Kurths, Recurrence plots for the analysis of complex systems. Phys. Rep. **438**, 237–329 (2007). https://doi.org/10.1016/J.PHYSREP.2006.11.001
29. C.L. Webber, J.P. Zbilut, Recurrence quantification analysis of nonlinear dynamical systems, in *Tutorials in Contemporary Nonlinear Methods for the Behavioral Sciences*, ed. by M. Riley, G. Van Orden (pp. 26–94). USA: National Science Foundation (2005)
30. R.V. Donner, Y. Zou, J.F. Donges, N. Marwan, J. Kurths, Recurrence networks—a novel paradigm for nonlinear time series analysis. New J. Phys. **12**, 33025 (2010). https://doi.org/10.1088/1367-2630/12/3/033025
31. R.V. Donner, J. Heitzig, J.F. Donges, Y. Zou, N. Marwan, J. Kurths, The geometry of chaotic dynamics—a complex network perspective. Eur. Phys. J. B **84**(4), 653–672 (2011). https://doi.org/10.1140/epjb/e2011-10899-1
32. N. Marwan, J.F. Donges, Y. Zou, R.V. Donner, J. Kurths, Complex network approach for recurrence analysis of time series. Phys. Lett. A **373**(46), 4246–4254 (2009). https://doi.org/10.1016/j.physleta.2009.09.042
33. G. Contopoulos, M. Harsoula, Stickiness effects in conservative systems. Int. J. Bifurc. Chaos **20**(7), 2005–2043 (2010). https://doi.org/10.1142/S0218127410026915